Intrinsic temporal tuning of neurons in the optic tectum is shaped by multisensory experience

Silas E. Busch[1], Arseny S. Khakhalin[1,*]

1 Biology Program, Bard College, Annandale-on-Hudson, NY.

* Correspondence: khakhalin@bard.edu

Abstract

Homeostatic intrinsic plasticity is often described as an adjustment of neuronal excitability to maintain stable spiking output. Here we report that intrinsic plasticity in the tectum of Xenopus tadpoles also supports temporal tuning, wherein neurons independently adjust spiking responses to fast and slow patterns of synaptic activation. Using the dynamic clamp technique, and five different types of visual, acoustic, and multisensory conditioning, we show that in tadpoles exposed to light flashes, tectal neurons became selective for fast synaptic inputs, while neurons exposed to looming and multisensory stimuli remained responsive to longer inputs. We also report a homeostatic co-tuning between synaptic and intrinsic temporal properties in tectal cells, as neurons that naturally received fast synaptic inputs tended to be most responsive to long-lasting synaptic conductances, and the other way around. These results expand our understanding of plasticity in the brain, and inform future work on the mechanisms of sensorimotor transformation.

Significance statement

With the recent explosion of work in neural connectivity reconstruction and biologically inspired deep learning, most researchers concentrate on the topology of connections between neurons, rather than on differences in neuronal tuning. Here we show that in a sensory network in Xenopus tadpoles, different neurons are tuned, and respond stronger, to either short or long synaptic inputs. This tuning tended to be opposite to the actual dynamics of synaptic inputs each cell received, such that neurons that normally receive shorter inputs generated stronger spiking in response to longer testing currents, and the other way around. This observation shows that even in networks that don't generate oscillations, neurons reshape their temporal selectivity, to optimize their impact on distributed calculations.

Introduction

It is often assumed, in fields as diverse as connectomics and machine learning, that the main difference between functional and dysfunctional neural networks lies in their connectivity (Takemura, 2014; Hildebrand et al., 2017; Bassett and Sporns, 2017; Reimann et al., 2017). Biological neurons, however, are tuned in ways that go well beyond adjusting one "strength" value per synapse: cells within the same network often demonstrate variability of activation thresholds (Kole and Stuart, 2012), production of bursts (Popovic et al., 2011), inactivation by strong inputs (Bianchi et al., 2012), and more. This diversity of tuning relies on coordinated changes of many parameters across a complex, multivariate landscape (O'Leary et al., 2013), as neuronal phenotypes are shaped by sensory experiences, and adjusted by modulatory inputs (Evans et al., 2015). The dysregulation of

intrinsic plasticity affects network dynamics (Tien and Kerschensteiner, 2018), and can lead to a loss of function (Marcelin et al., 2009). And yet, with the obvious exception of oscillatory networks (Marder and Taylor, 2011; Picton et al., 2018), for many brain areas it is still unclear whether variation of intrinsic phenotypes serves as a defining aspect of network topology and architecture, or whether it is just a consequence of transfer function normalization (Titley et al., 2017).

The optic tectum of the *Xenopus* tadpole is an ideal model for exploring these questions: it is a highly malleable distributed network of about 10^4 neurons (Pratt and Khakhalin, 2013), involved in stimulus discrimination and sensorimotor transformations (Dong et al., 2009; Khakhalin et al., 2014). In development, tectal neurons acquire diverse intrinsic and synaptic phenotypes that are also shaped by sensory experiences (Xu et al., 2011; Ciarleglio et al., 2015). Circuits in the tectum can learn and reproduce the temporal dynamics of inputs to which they were exposed (Pratt et al., 2008): a property that could in principle be achieved through synaptic changes alone (Lukoševičius and Jaeger, 2009), but which is more likely to involve intrinsic temporal tuning (Narayanan and Johnston, 2008; Beatty et al., 2014). Finally, tectal neurons exhibit strong Na channel inactivation, which seems to play a role in collision detection (Jang et al., 2016), and is one of the targets for intrinsic plasticity (Bianchi et al., 2012).

In this study, we asked two specific questions about the properties of intrinsic plasticity in tectal networks. First, we asked whether intrinsic plasticity is limited to changes in excitability, or whether it is more nuanced and can differentially adjust neuronal responsiveness to inputs with different dynamics. Second, we checked whether changes in intrinsic properties in the tectum are a homeostatic response to each cell's history of synaptic activation, or if they are independent of synaptic properties. In our previous large-scale census of tectal cells (Ciarleglio et al., 2015), we observed no interaction between intrinsic and synaptic phenotypes, and despite an extensive search, we did not detect signs of temporal tuning (ibid, figures 2, 4). However, we propose that the standard current-clamp protocols used in previous studies (Pratt and Aizenman, 2007; Hamodi and Pratt, 2014) were not adequate to detect important changes in the function of voltage-gated channels (see Discussion).

Here we show that the intrinsic plasticity of tectal neurons goes beyond changes in average spikiness and supports temporal selectivity that can be reshaped by sensory experience. Furthermore, we show that the tuning of intrinsic properties is coordinated with the duration of synaptic inputs received by each cell. These results rely on two methodological innovations. First, instead of using current injections, we employed the dynamic clamp technique, which allowed a more realistic simulation of synaptic conductances (Prinz et al., 2004a). Unlike more common voltage and current clamp techniques, in dynamic clamp the electric current injected into the cell is dynamically adjusted, based on a predefined formula that depends on cell membrane potential and time. Second, instead of relying on one type of sensory stimulation, we used five different stimulation protocols and compared their effects on intrinsic tuning. The use of different sensory modalities also gave us insight into an unrelated, but equally intriguing question of multisensory integration in the brain (Deeg et al., 2009; Felch et al., 2016; Truszkowski et al., 2017), as for the first time we were able to look at tectal network retuning in response to multisensory stimuli in freely behaving tadpoles.

Results

All analysis scripts and summary data for every cell can be found at:
`https://github.com/khakhalin/Dynamic-clamp-2018`

Changes in excitability in response to sensory stimulation

Our first question was whether our stimulation protocols caused changes in intrinsic excitability of tectal neurons. From previous studies, we knew that in tadpoles exposed to four hours of LED flashes, tectal neurons became more excitable (Aizenman et al., 2003; Ciarleglio et al., 2015). However, the stimuli we used in the present study were weaker, and similar to those used in behavioral experiments (Khakhalin et al., 2014; James et al., 2015; Truszkowski et al., 2017). We presented a checkerboard pattern that inverted once a second either instantaneously (Figure 1C left, dubbed “Flash”), or with a slow transition over the course of a second (old black squares shrank to white, while new black squares grew from old white squares; Figure 1C right; dubbed “Looming”; see Methods).

After conditioning, we excised the brain, obtained whole cell patch clamp recordings from neurons in the tectum (Figure 1A), and counted spikes produced during dynamic clamp in response to simulated synaptic conductances of different durations and amplitudes (Figure 1B). We used conductances of 4 different durations (100, 200, 500, and 1000 ms), and 3 different amplitudes (peak conductances of 0.2, 0.5, and 1.0 nS), matching the range of synaptic currents observed in tectal circuits *in vivo* (see Methods). Contrary to our expectations, in tadpoles that were exposed to instantaneous checkerboard inversions (flashes), tectal neurons on average became not more, but less spiky, and generated 0.4 ± 0.4 spikes, across all types of dynamic clamp inputs, compared to 0.9 ± 1.0 spikes in control (Figure 1D, left column; $F(1,677)=30.4$, $p=5e-8$, n cells=28, 29. Here and below, F-values are reported for a multivariate fixed effects analysis of variance with selected interactions, where cell id is used as a repeated measures factor; see Methods for a detailed description). Neurons exposed to looming transitions also spiked less than control neurons (0.6 ± 0.4 spikes; $F(1,629)=9.6$; $p=0.002$; n=28, 25), but more than those exposed to instantaneous ”flashes” ($F(1,641)=3.7$; $p=4e-6$; n=29, 25), which was likewise unexpected. In the tadpole tectum, looming stimuli are known to elicit stronger responses compared to instantaneous inversions (Khakhalin et al., 2014), yet the suppression yielded by looming stimuli was weaker.

We then mapped the amplitude tuning of neurons (amplitude transfer function, or gain), by looking at how an increase in transmembrane conductance translated into increased spike output. Compared to control, neurons from animals exposed to visual stimuli had a flatter amplitude tuning curve (Fig 1D,E), and did not increase their spiking as fast in response to larger conductances ($F(1,677)=15.9$, $p=8e-5$; and $F(1,629)=8.3$, $p=0.004$ for flash- and looming transitions respectively). The flattening of response curves seemed slightly more pronounced for flashes than for looming, but this difference was not significant ($F(1,641)=3.5$; $p=0.06$).

These results show that prolonged stimulation had an effect on intrinsic excitability, but its direction was opposite to what was previously described (Aizenman et al., 2003; Ciarleglio et al., 2015), as neurons became less excitable. Moreover, while looming stimuli are known to be more salient, both behaviorally and physiologically (Khakhalin et al., 2014), they had a weaker long-term effect on neuronal excitability in comparison to less salient flashes. We conjecture that the difference in the direction of change is due to our stimuli being weaker than those used in earlier studies (see Discussion), and we further explore the difference between flashes and looming stimuli below.

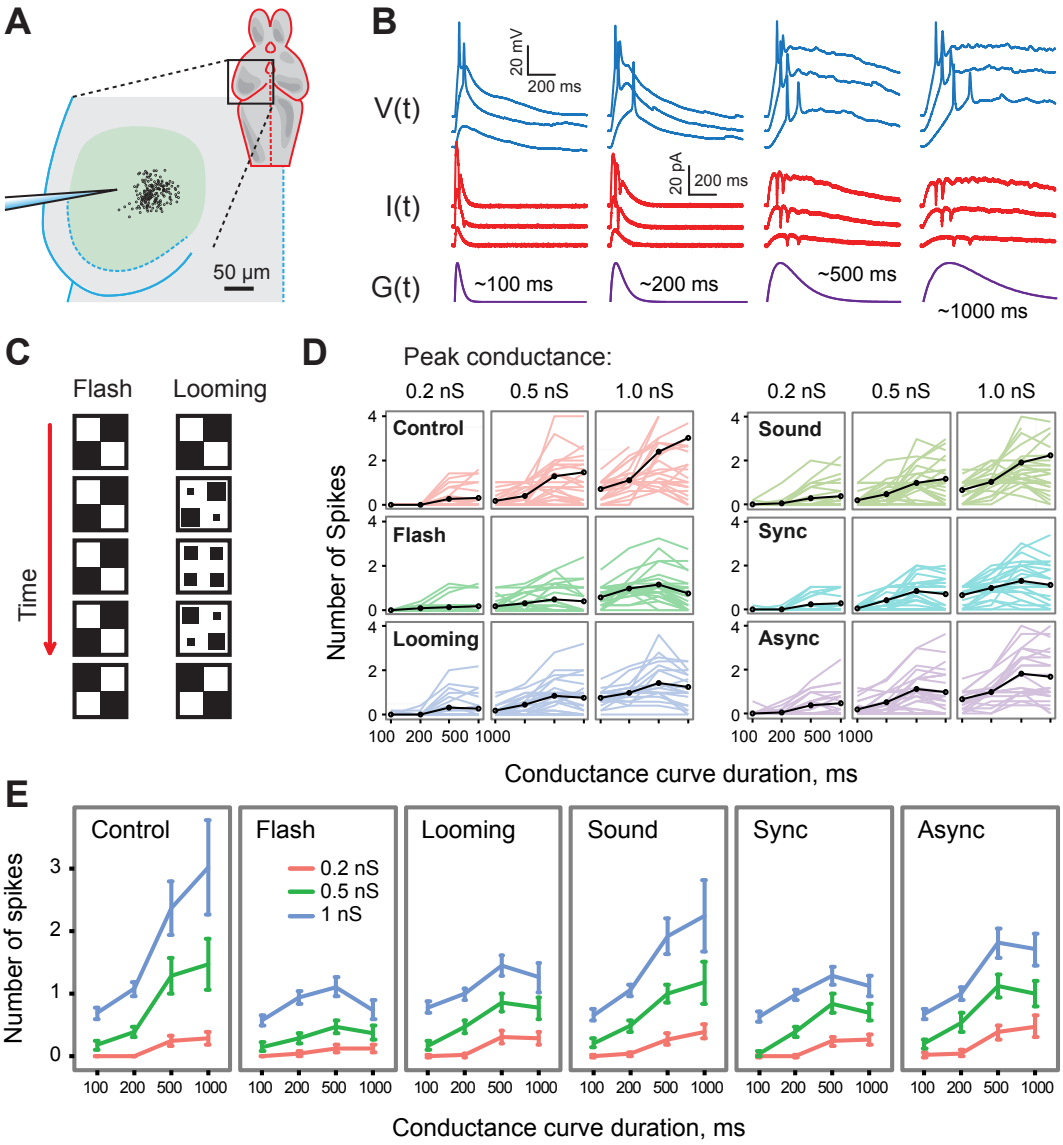

Figure 1. Overview of experimental design and summary of dynamic clamp results. (**A**). Positions of tectal neurons that were recorded. (**B**). Sample data from a dynamic clamp experiment. Bottom row: the dynamics of conductances G(t) of four different durations simulated by the dynamic clamp system. Middle row: the currents I(t) dynamically injected into a cell based on conductances of 4 different durations and 3 different amplitudes. Top row: resulting voltage traces V(t) that were recorded and analyzed. (**C**). A schematic of visual conditioning in "Flash" (left) and "Looming" (right) groups. (**D**). The number of spikes produced by all neurons in all experiments, split by input peak conductance, and plotted against conductance duration. Black lines show respective averages. (**E**). A summary of data from D, presented as averages and 95% confidence intervals.

Changes in intrinsic temporal tuning

We then examined whether different types of sensory activation would differentially reshape temporal intrinsic tuning in tectal neurons. As changes in intrinsic properties seemed homeostatic (increased activation led to reduced spiking), by the same logic, one could expect shorter stimuli (flashes) to selectively suppress responses to shorter synaptic inputs. Alternatively, shorter stimuli could reshape the network, making neurons better adjusted to working with short bursts of activation, as previously described for synaptic processing (Aizenman and Cline, 2007) and recurrent activity in the tectum (Pratt and Aizenman, 2007; Shen et al., 2011).

Across input conductances of different lengths (100, 200, 500, and 1000 ms), neurons exposed to flashes and looming stimuli responded differently than in control ($F(1, 677)=25.1$; $p=7e-7$; and $F(1,629)=12.0$; $p=6e-4$ respectively). In control neurons, longer inputs typically evoked stronger spiking, whereas neurons from stimulated animals had flatter tuning curves, with a plateau, or even a decrease in spike number for longer conductance injections (Figure 1E). In essence, while control neurons “preferred” longer inputs, stimulated neurons developed a preference for shorter synaptic inputs, and this change was more pronounced in neurons exposed to flashes than in those exposed to looming stimuli ($F(1,641)=7.5$; $p=0.006$). This suggests that the change in overall intrinsic excitability, and the change in temporal tuning, follow two different kinds of logic. The overall excitability is homeostatic, as neurons became less excitable in response to stronger stimulation. The temporal retuning however can be better described as “adaptive”, as neurons exposed to shorter stimuli (flashes) became relatively *more* responsive to shorter stimuli, and less responsive to longer stimuli, which is the opposite of what one would expect for a purely homeostatic retuning. We chose to call this type of plasticity ”adaptive”, as presumably it means that after exposure to faster stimuli, neurons become more equipped to process faster patterns of activation (Stemmler and Koch, 1999).

Effects of acoustic and multisensory stimulation

While the optic tectum (homologous to superior colliculus in mammals) is often described as a primarily visual area, it is also involved in heavy multisensory computations (Stein et al., 2014). In tadpoles, it integrates visual information with inputs from mechanosensory, auditory, and lateral line modalities (Deeg et al., 2009; Pratt and Aizenman, 2009; Hiramoto and Cline, 2009; Felch et al., 2016; Truszkowski et al., 2017), but the logic of this integration is still unclear. We wondered whether acoustic stimuli would reshape intrinsic properties of tectal neurons, and whether this retuning would be similar to that produced by visual stimuli.

To test this question, we exposed tadpoles to four hours of behaviorally salient “click” sounds (James et al., 2015; Truszkowski et al., 2017), provided at the same frequency (every second) as visual stimuli in the first set of experiments. We found (Fig 1D, E) that exposure to startle-inducing sounds (group “Sound”) did not lead to significant changes in either average spikiness (0.8 ± 0.7 spikes; $F(1,689)=1.7$; $p=0.2$; $n=28, 30$), amplitude transfer function ($F(1,689)=2.0$; $p=0.2$), or temporal tuning curve ($F(1,689)=2.0$; $p=0.2$). This suggests that acoustic stimuli did not strongly activate tectal circuits during conditioning, despite being more behaviorally salient (for our stimuli, at the onset of stimulation, acoustic clicks evoked startle responses in about 50-80% of cases, compared to 5-10% for checkerboard inversions (James et al., 2015; Truszkowski et al., 2017)). As one possible explanation, auditory and mechanosensory inputs may have different cellular or subcellular targets in the tectum (Bollmann and Engert, 2009), or they may differentially recruit tectal

inhibitory circuits (Liu et al., 2016; Hamodi et al., 2016).

We then combined visual and acoustic stimuli in two different ways and looked at the effects of multisensory stimulation on the intrinsic properties of tectal neurons. For some animals, we synchronized the instantaneous checkerboard inversions (flashes) with sound clicks (dubbed “Sync”), while for others we staggered visual and acoustic stimuli by half a period (500 ms; dubbed “Async”). We found (Fig 1D, E) that, after four hours of multisensory stimulation, tectal neurons were more excitable than after visual stimulation alone (0.6 ± 0.4 spikes, F(1,689)=11.2, p=8e-4; and 0.7 ± 0.6 spikes, F(1,665)=41.7, p=2e-10, for sync and async respectively, across all testing conditions). Compared to the “Flash” group, the tuning curves in multisensory groups were less flat, with a stronger effect in the Async group (for amplitude tuning: F(1,689)=1.3, p=0.3, and F(1,665)=2.4, p=0.02 in Sync and Async groups respectively; for temporal tuning: F(1,689)=9.3, p=0.002, and F(1,665)=22.8, p=2e-6 respectively). This suggests that on their own sound clicks had little effect on tectal excitability, but when added to visual flashes, sound clicks negated effects of retuning that visual stimulation would have had (Fig 2C).

Changes in average neuronal tuning, and tuning variability

To visualize and interpret differences in neuronal tuning, we quantified each of the three aspects of intrinsic tuning (average spikiness, amplitude tuning, and temporal tuning) with one value per neuron (see Methods). We used the mean number of spikes across all conditions as the measure of ”spikiness”; the linear slope of the number of spikes as a function of conductance amplitude as the measure of ”amplitude tuning”, and the quadratic term of the curvilinear regression for the number of spikes as a function of input duration as the value characterising the ”temporal tuning” or adaptation index of each neuron (Figure 2A). The numerical values of these ”tuning coefficients” are not easily interpretable, but they capture the character of tuning curves for each neuron (Figure 2A). All three parameters differed across experimental groups: F(5,160)=3.1, p=0.01 for average spikiness (Figure 2C; see Methods for model description); F(5,160)=4.8, p=4e-4 for amplitude tuning (Figure 2B); and F(5,160)=3.6, p=4e-3 for temporal tuning (Figure 2C).

A visual comparison of neuronal tuning in different experimental groups (Fig 2C) shows that acoustic stimulation had opposite effects when provided on its own (without visual stimulation) than when added to visual flashes. Compared to control neurons, cells exposed to sound had slightly lower amplitude tuning coefficients (flatter curve, Cohen’s $d=-0.29$), and more negative (curving down, $d=-0.27$) temporal tuning coefficients (Hotelling t-squared test p=0.2). When sounds were added to flashes, however, both transfer functions became less flat (d=0.65 and 0.26 for ”Async” compared to “Flash”, for amplitude and temporal tuning respectively), and more like curves for control neurons (Hotelling test p=0.04). Thus, acoustic stimulation tended to tune the network in the same direction as visual stimulation when delivered alone (Figure 2D), but negated the effect of visual stimulation when combined with it. This may imply that multisensory integration in the tectum is dominated by inhibition (see Discussion). Note also that looming stimuli seemed to have weaker effects on neuronal tuning compared to flashes, both in terms of amplitude (d=0.44) and temporal tuning (d=0.22).

Describing neuronal tuning with only a few variables allowed us to compare cell-to-cell variability of tuning in different experimental groups. We found that this variability decreased as neurons were modulated away from the baseline (Bartlett test p=2e-9 for amplitude tuning, p=1e-9 for temporal tuning; Figure 2D). Groups that were significantly different in average values also had different variances (F-test with $p<0.05$), such as Control vs. Flash

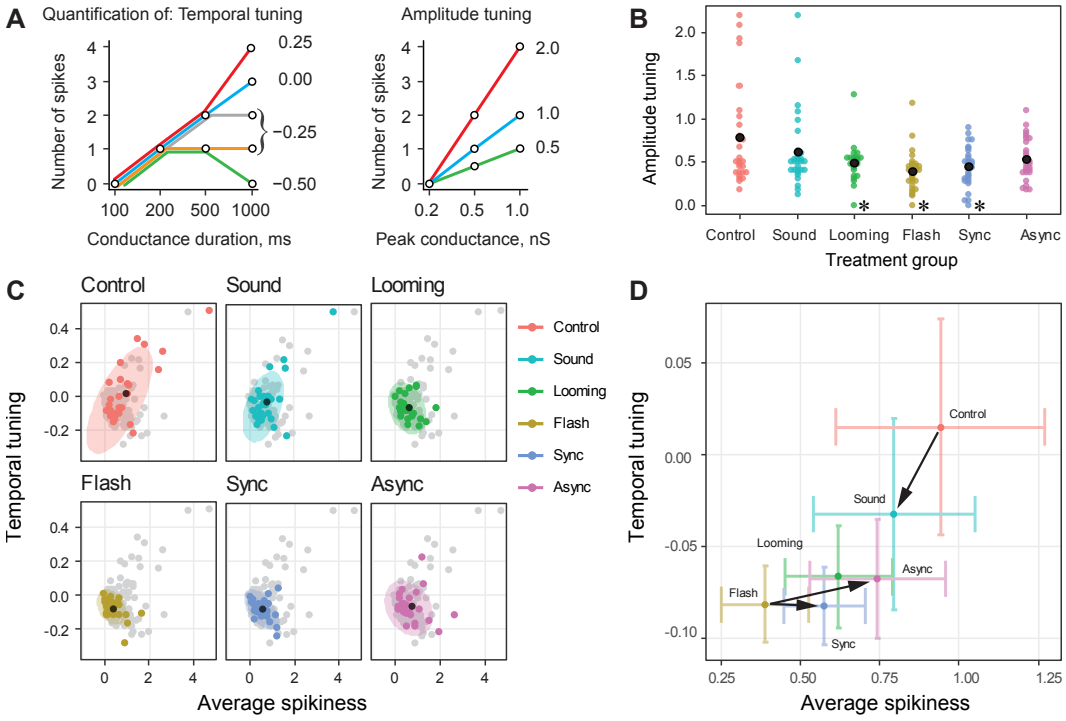

Figure 2. Quantification of changes in temporal tuning in response to sensory experience. (**A**). An illustration of how "Temporal tuning" and "Amplitude tuning" values were calculated. For the temporal tuning measure, the value of zero corresponds to linear dependency (blue line), positive values - to an accelerating, supralinear curve (red), and negative values - to a plateau-shaped curve (purple, yellow). For amplitude tuning, higher values correspond to faster increase in spiking with increased conductance. (**B**). Amplitude tuning of neurons across different experimental groups (stars show t-test $p<0.05$ compared to control). (**C**). Temporal tuning and average spikiness of neurons in different experimental groups; in each plot all neurons across all groups are shown in gray, while neurons from one target group are shown in color; means are shown as black dots; ellipses represent 95% normal confidence regions. Two outliers (top right corner) are brought within the axes limits. (**D**). Same data as in (C), shown as averages for each group, with 95% confidence intervals. Black arrows show the effects of sound clicks, when they were added to control, and when they were added to "Flashes" to form two types of multisensory stimuli.

and Control vs. Looming for both amplitude and temporal tuning. This expands on a finding in our previous study (Ciarleglio et al., 2015) that prolonged patterned stimulation reduces diversity of tuning profiles in the network, reshaping them according to the spatiotemporal characteristics of the stimulus, with stronger stimuli having stronger effects on tuning diversity.

Changes in synaptic properties

To see whether prolonged sensory stimulation affected synaptic inputs received by tectal neurons, we recorded evoked excitatory postsynaptic currents in response to optic chiasm stimulation. We found that the amplitude of the early, monosynaptic component of evoked responses (the average current between 5 and 15 ms after the shock; Figure 3B) differed

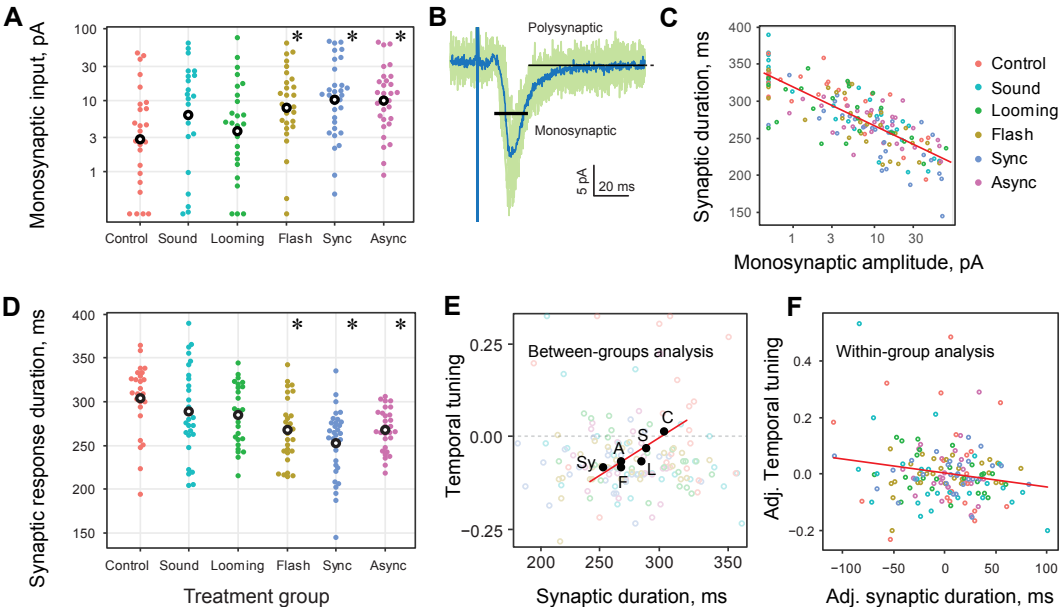

Figure 3. Changes in synaptic transmission, and co-tuning of synaptic and intrinsic neuronal properties. (**A**). Amplitudes of early monosynaptic inputs to tectal neurons in all experimental groups (in log scale, outliers brought within the axes limits, stars show t-test $p<0.05$ compared to control). (**B**). A sample synaptic recording, showing all traces for one cell (green) and an average trace (blue). The black bars show the areas at which early monosynaptic and late polysynaptic currents were measured; the vertical position of each bar represents the respective average current. The second, longer bar does not completely fit within the figure at this scale. (**C**). Synaptic current duration (vertical axis) was mostly defined by the amplitude of early monosynaptic inputs (horizontal axis). (**D**). Synaptic current durations were different between experimental groups (see text; stars show t-test $p<0.05$ compared to control). (**E**). Across experiments, average temporal tuning in each group positively correlated with the average durations of synaptic currents they received. (**F**). Within experimental groups, temporal tuning of individual neurons negatively correlated with the duration of synaptic currents they received. Axes show within-group deviations of temporal tuning and synaptic current duration from respective averages for each group.

across experimental groups (Figure 3A; $F(5,161)=3.2$, $p=0.009$; see Methods for a description of the linear model we used). Both Sync and Async multisensory groups had larger early synaptic currents than the Control group (Tukey $p=0.03$ and 0.04; Cohen $d=0.92$ and 0.73 on log-transformed data respectively). The amplitude of late synaptic currents–produced by recurrent network activation (15-145 ms after the stimulus)–did not differ across groups.

To better match and compare temporal properties of synaptic inputs to those of intrinsic tuning, we calculated average "synaptic current duration" for each cell as a temporal "center of mass" of currents within the first 700 ms after optic chiasm stimulation (see Methods). Neurons with different contribution of early and late synaptic responses naturally had different synaptic current duration: cells with strong monosynaptic inputs had shorter currents, while polysynaptic activity made synaptic currents longer (Figure 3C; $p=2e\text{-}16$, $r=-0.78$, $n=168$). The synaptic current duration was different across treatment groups (Figure 3D; $F(5,163)=6.3$, $p=2e\text{-}5$). Cells in Flash, Sync, and Async groups all received shorter synaptic inputs than Control cells (Tukey $p<0.05$, mean duration of 267 ± 36,

253±39, 268±24, and 304±40 ms, respectively), indicating that prolonged sensory activation with short, frequent stimuli reshaped synaptic transmission in the tectum, making it faster through selective potentiation of visual inputs from the eye.

Co-tuning of synaptic and intrinsic properties

To see whether intrinsic and synaptic temporal properties of tectal cells coordinated with each other, we compared intrinsic temporal tuning of every neuron (that is, whether it preferred longer or shorter simulated synaptic inputs in dynamic clamp experiments) to the actual duration of synaptic inputs it received during in-vitro stimulation of the optic chiasm. We found that, on average, cells exposed to stronger sensory stimuli preferred shorter synaptic inputs in dynamic clamp and also received shorter synaptic currents during optic chiasm stimulation, leading to a positive correlation between average synaptic and intrinsic properties for each group (Figure 3E; r=0.89, p=0.02, n=5). This means that *between* treatment groups, changes in synaptic and intrinsic properties were adaptively coordinated, and the stronger the average change in synaptic transmission, the more cells reshaped their intrinsic properties to adjust to this change.

In contrast, *within* experimental groups, cells that preferred shorter synaptic inputs in dynamic clamp tended to receive longer synaptic currents, and vice versa ($F(1,145)=4.9$, $p=0.03$). We calculated differences between the properties of each individual cell and the average for the experimental group to which it belonged, and showed these deviations from respective averages on one plot (Figure 3F). Cells that had shorter synaptic currents, compared to other cells in their group, tended to be selective for longer synaptic inputs in dynamic clamp (adjusted $r=-0.19$, $p=0.02$, $n=151$). This means that individual neurons tended to tune their intrinsic properties away from the typical statistics of their inputs, decreasing their responses to common input patterns, and enhancing responses to unusual patterns of synaptic activation.

Note that the correlation of intrinsic and synaptic properties had opposite signs between-groups (positive) and within-groups (negative), so if we lumped all cells from all groups together, we would have found no correlation between these two variables ($r=-0.07$, $p=0.4$, $n=151$). This is a textbook example of ”Simpson’s paradox”, wherein a pattern holds within subgroups, but disappears or is reversed on a full set because of pronounced differences between groups.

For amplitude tuning, the interaction between synaptic and intrinsic parameters of tectal cells was inconclusive. The amplitude of early synaptic responses and intrinsic amplitude tuning formally correlated on a full dataset ($p=0.03$, $r=-0.17$, $n=151$), but the correlation disappeared ($p>0.05$) when the highly non-normal amplitude data was log-transformed, or when 4 extreme values (out of 135 total) were removed. When analyzed separately, the between-groups and within-groups correlations were also insignificant. A similar analysis for amplitudes of late synaptic currents also did not yield reliable results.

The mechanisms behind temporal intrinsic plasticity

Knowing that tectal neurons can tune to inputs of different temporal dynamics, we then tried to identify the cellular mechanisms underlying this tuning. For each cell, we used a sequence of voltage steps (Figure 4A) to activate Na and K conductances, and quantified ionic current amplitudes and activation potentials (Figure 4B) as it was done in earlier

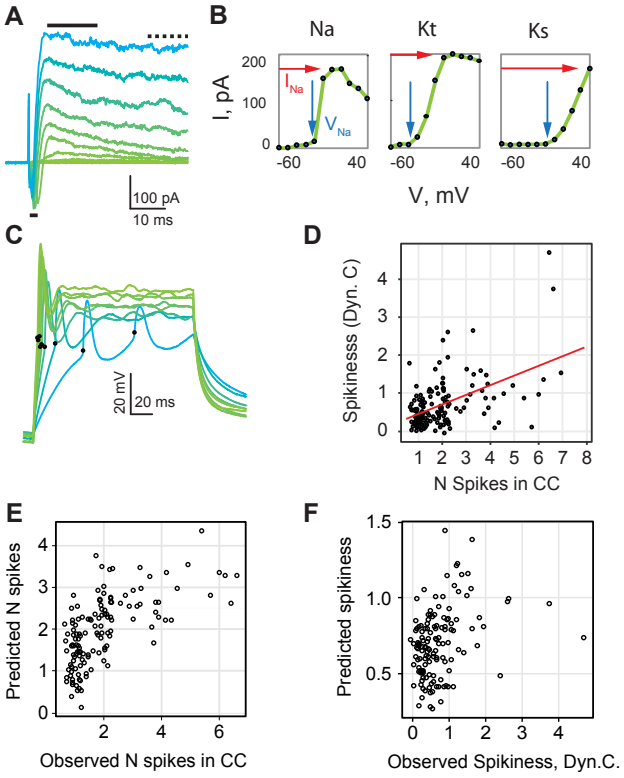

Figure 4. Electrophysiological properties of individual neurons compared to their spiking in current and dynamic clamp experiments. (**A**). A set of curves from one voltage step experiment; black bars show the areas used to average Na (bottom) and transient K (top) currents (see Methods). (**B**). Processing of ionic currents data with IV-curves translated into two parameters (threshold potential and peak current) for each ionic conductance. (**C**). Sample data from one current clamp experiment; spikes are marked with black dots. (**D**). Estimations of spikiness from current clamp experiments (horizontal axis) and dynamic clamp experiments (vertical axis) correlate. (**E**). The number of spikes registered in current clamp mode: values predicted from a linear model plotted against observed values. The model works reasonably well (61% of variance explained). (**F**). Similar comparison for the dynamic clamp experiments: the model has very low predictive value (13% of variance explained). Here and in E, both values are adjusted for position.

studies (Ciarleglio et al., 2015). Together with cell membrane resistance (Rm) and capacitance (Cm) it gave us eight intrinsic parameters for every cell: peak amplitudes for sodium current, early (transient) potassium current, and late (stable) potassium current (INa, IKt, IKs respectively), and activation potentials for these three currents (VNa, VKt, and VKs).

We ran a stepwise generalized linear model selection analysis (R package stepAIC, Venables and Ripley 2013) to explain the intrinsic tuning of cells recorded in all experimental groups through these eight variables. We found that the average spikiness (after compensation for position within the tectum; see Methods) was best described by a combination of sodium peak current (INa) and membrane resistance (Rm) variables, but these variables explained only 8% and 2% of cell-to-cell variance respectively ($F(1,130)=11.3$, and $F(1,130)=4.5$; Figure 3E). Together, all eight cellular parameters described only 13% of variance in average spikiness. The temporal tuning value was best explained by sodium current activation potential and membrane resistance (VNa: 7%,

F(1,147)=10.7; Rm: 2%, F(1,147)=3.1), with all eight variables explaining only 11% of total variance. For amplitude tuning, the proposed best model included peak sodium current (INa: 6%, F(1,163)=10.0) and sodium activation potential (VNa: 2%, F(1,1,163)=3.5), with all eight variables accounting for 10% of variance. This very low total explained variance suggests that while ionic currents and their activation potentials clearly affected intrinsic tuning of tectal cells, most cell-to-cell variability in intrinsic phenotypes stemmed from some other properties that were different between cells. In agreement with this assessment, the effect of experimental group on either mean spiking, temporal, or amplitude tuning curves remained significant even after compensating for all 8 intrinsic properties (sequential sum of squares analysis of variance p=0.03, 0.001, and 0.003 respectively), suggesting that changes in tuning across experimental groups was mediated by other factors.

A comparison between dynamic clamp and current clamp experiments

The inability to predict spiking of tectal neurons through their isolated electrophysiological properties was unexpected, and stood in a seeming contradiction with our previous study (Ciarleglio et al., 2015). Fortunately, in the current study, we recorded spiking traces in response to “classic” current steps (Figure 4C), which allowed a direct comparison between the results of current clamp and dynamic clamp protocols. Across all cells, the maximal number of spikes observed during current step injections correlated with the average number of spikes in dynamic clamp experiments (Figure 4D; r=0.46, p=2e-9, n=152). In agreement with (Ciarleglio et al., 2015), spiking in current clamp experiments correlated with peak sodium (INa: r=0.42, p=2e-8, n=152) and stable potassium currents (IKs: r=0.39, p=2e-7), as well as activation potential for sodium current (VNa: r=0.24, p=0.02). Overall, the 8 intrinsic variables described above (Rm, Cm, three peak currents, and three activation potentials) explained 61% of cell-to-cell variability in the maximal number of spikes from current clamp experiments (Figure 4E), comparable to 49% reported in our previous study (Ciarleglio et al., 2015), and noticeably higher than 13% for dynamic clamp experiments (Figure 4F).

We can therefore conclude that our set of eight cellular parameters can better predict spiking during current step injections (61% of variance) than in dynamic clamp experiments (13% of variance). This suggests the existence of internal properties that strongly affect spiking in dynamic clamp experiments, but are inaccessible through standard current and voltage step protocols (see Discussion). Our hypothesis is indirectly supported by two more observations: that of the eight cellular parameters only one was significantly ($p<0.05$) different across treatment groups (NaV: F(5,175)=3.7, p=0.003), and that the number of spikes detected in current clamp experiments did not differ across experimental groups (F(5,165)=0.8, p=0.6).

Effects of position within the tectum

In all analyses presented above, we adjusted cell properties for rostro-caudal and medio-lateral position of each cell within the tectum, as in tadpoles both intrinsic (Hamodi and Pratt, 2014) and synaptic properties (Wu et al., 1996; Khakhalin and Aizenman, 2012) are known to differ between older (rostro-medial) and younger (caudal, lateral) parts of the developing tectum. In this study, most cell properties we measured correlated ($p<0.05$, after correction for treatment group differences) with either medial or rostral position within the tectum (medial: membrane capacitance r=−0.17, membrane resistance r=0.25, sodium current activation potential r=−0.30, stable potassium current r=−0.16, early synaptic

amplitude r=−0.22, synaptic current duration r=0.29; rostral: peak sodium current r=0.18, late synaptic amplitude r=0.11; n between 168 and 183). Curiously, neither of the three measures of intrinsic tuning (average spikiness, temporal tuning, and amplitude tuning) correlated with position ($p>0.1$, n=168). This may suggest that while low-level properties of tectal cells depended on their age, their spiking phenotypes were largely age-independent. Thus, different cells seemed to achieve similar spiking behaviors through different combinations of underlying parameters, relying on the principle of "parameter degeneracy" (Prinz et al., 2004b; Drion et al., 2015).

Discussion

In this study we show that different sensory stimuli retuned neurons in the optic tectum of *Xenopus* tadpoles in different ways, thereby inducing changes in both their temporal tuning and amplitude transfer functions. This addresses our first question about the functional scope of intrinsic plasticity in the optic tectum, and shows that it goes well beyond simple adjustments of neuronal spikiness.

As our technical resources were rather limited, in this study we don't explicitly address the mechanisms of this newly discovered intrinsic temporal tuning. We can, however, offer two working hypotheses that may explain these results. As tadpole tectal cells don't express "true" resonance currents, such as h-currents (Ciarleglio et al., 2015), most temporal tuning effects we observed seem to be due to differences in ionic current inactivation in different cells. One obvious way of tuning ionic channel inactivation would be for every cell to modulate sodium or transient potassium currents via channel phosphorylation, or by changing the expression of different channel variants, to shift their inactivation dynamics (Frank and Catterall, 2003; Goldwyn et al., 2018). To test this hypothesis, one would need to induce changes in temporal tuning similarly to how we did in this paper, pharmacologically isolate different ionic currents, and directly measure their inactivation dynamics.

Another hypothetical mechanism that can underlie our current results is inspired by a yet unexplained finding from our earlier study (Ciarleglio et al., 2015): namely, that one of the key electrophysiological parameters regulating excitability of tectal cells is cell membrane capacitance (Cm). Traditionally, cell capacitance is thought of as a relatively immutable parameter that describes cell morphology, and can even be used to estimate its size. Yet, in the tadpole tectum, we found it to drop both with age and after strong sensory stimulation, even though cells don't seem to change their visual appearance (Ciarleglio et al. 2015, Figure 7D). An intriguing possibility is that these changes in cell capacitance may be due to electric uncoupling of three major compartments of *Xenopus* tectal cells: their dendritic tree, soma, and axon initial segment (Bollmann and Engert, 2009; Jarvis et al., 2018). This differential uncoupling may be achieved through either minor changes in cell morphology (Leterrier, 2018), or through target modulation of sodium and potassium channels at key points between the compartments, which would introduce shunting, and so strongly affect cell excitability (Grubb and Burrone, 2010; Kuba et al., 2010). One way to test this hypothesis could be to perform immunostaining of cleared tectum preparation after sensory stimulation, and if any changes in the distribution of sodium and potassium channels is discovered, to validate the effect of these changes in a computational model.

In answer to our second question about whether intrinsic and synaptic properties of tectal cells are in any way coordinated, here we show that intrinsic and synaptic temporal properties are co-tuned in the tectum, and moreover, that this co-tuning can be modified by sensory experience. In contrast with earlier studies that report increased excitability post-stimulation (Aizenman et al., 2003; Dong et al., 2009; Ciarleglio et al., 2015), we found that sensory stimulation led to a suppression of spiking. The reason for that, most probably,

is that the visual stimulation used in earlier studies was provided with a LED box, which was so bright and of so high contrast that it caused a suppression of retinal synaptic inputs via a polyamine block of AMPA receptors (Aizenman et al., 2003). This suppression then triggered a “second-order” homeostatic compensation (Turrigiano, 2011; Tien and Kerschensteiner, 2018), making neurons spikier. In our current experiments, however, synaptic inputs were not suppressed, and neuronal activation during sensory conditioning was stronger than in control, causing a decrease in intrinsic spikiness.

Our study described an important difference between dynamic clamp results (that were affected by stimulation, but could not be explained through low-level intrinsic parameters) and the results obtained in ”classical” slow clamp experiments (that were not affected by stimulation, yet better coordinated with intrinsic parameters). This difference may be interpreted in two ways. One possible interpretation is to assume that dynamic clamp in the soma provided a bad approximation of peripheral synaptic inputs, as space clamp error is more pronounced for fast voltage fluctuations than for constant current injection (Spruston et al., 1993; Prinz et al., 2004a). We find this hypothesis unlikely, however, as dynamic clamp responses were consistently different in animals with different sensory history, which suggests, at the very least, that we have captured some important aspects of intrinsic diversity, even if our estimations were biased.

Alternatively, and in our opinion more likely, intrinsic excitability of tectal cells is affected by properties that are not easily accessible by standard slow voltage and current clamp protocols, such as axon initial segment relocation, or targeted modulation of axonal voltage-gated channels we described above (Grubb and Burrone, 2010; Kole and Stuart, 2012). In cells with excitable dendrites, channels of the axon initial segment may constitute only a small fraction of all voltage-gated channels, yet have a disproportionately large effect on the spiking output of the cell, and on its temporal tuning (Kole et al., 2007; Hamada et al., 2016). Furthermore, prolonged current injections in the soma are likely to quickly inactivate transient channels in the axon, obscuring any possible interplay between action potential width and Na channel recovery during burst firing (Popovic et al., 2011; Kole and Stuart, 2012). Conversely, this effect would still affect spiking in more realistic, fast dynamic clamp experiments.

Our findings lead to several verifiable predictions. As rapid inactivation of spiking in tectal neurons plays a role in collision detection (Khakhalin et al., 2014; Jang et al., 2016), a change in temporal tuning should affect collision detection dynamics, which can be verified experimentally. More specifically, we predict that a visual stimulation that retunes neurons to faster stimuli (Flash) would make tadpoles selectively less responsive to slow collisions, and increase the latency of collision avoidance due to non-linear dynamics of retinal activation for realistic looming stimuli that are slow in the beginning and fast towards the end (Jang et al., 2016). These changes in intrinsic temporal tuning would also reshape the connectivity of tectal networks, as fast-inactivating cells would not support short recurrent loops within the network, thus promoting long-ranged polysynaptic connectivity (Fiete et al., 2010; Clopath et al., 2010). Finally, based on the multisensory phenomena reported in this paper, we predict that even though multisensory stimulation tends to increase tectal responses in vitro (Felch et al., 2016; Truszkowski et al., 2017), it would be likely to reduce peak activation in vivo.

To sum up, we present a novel case of temporal selectivity in non-oscillatory neurons in a distributed sensory network, and demonstrate that intrinsic temporal tuning of neural cells correlates with their synaptic properties. It is particularly interesting that the temporal co-tuning we observed was homeostatic in nature, as cells tended to be selective for inputs of dynamics they did not usually experience. We hypothesize that this adjustment of temporal tuning is the reason why this tuning was so easily disrupted by strong visual

stimulation, when for a few hours we drastically changed the statistics of inputs received by every cell. Tuning to "unusual stimuli" at the level of individual neurons fits into the narrative of information transfer maximization (Stemmler and Koch, 1999; Brenner et al., 2000) and network criticality (Rubinov et al., 2011), wherein every element of a network tries to locally maximize its influence over the overall computation. This may have intriguing consequences for the function and development of sensory networks in the brain, which can be further probed by computational modeling (Khakhalin et al., 2014; Jang et al., 2016), and verified experimentally. We also suspect that any cell with a sufficiently large dendritic tree would be able to tune its temporal intrinsic selectivity the way we describe. We expect that in most cases these changes would not be noticeable in experiments with standard voltage- and current-clamp protocols, but can be probed with a dynamic clamp technique. It would therefore be very interesting to see whether our results will replicate in other sensory systems, such as the mammalian cortex.

Acknowledgements

We would like to thank Carlos Aizenman (Brown University), Justin Hulbert (Bard College), and Kara Pratt (University of Wyoming) for their feedback on drafts of this paper. Part of this work was supported by the Bard Summer Research Institute (BSRI) program.

The authors have no conflicts of interest to disclose.

Author Contributions

S.E.B.: Conception and design, acquisition of data, analysis and interpretation of data, drafting and revising the article.

A.S.Kh.: Conception and design, analysis and interpretation of data, figure preparation, drafting and revising the article.

Materials and Methods

Housing and sensory conditioning

All experimental protocols were in accordance with Bard College Institutional Animal Care and Use Committee (IACUC), and National Institutes of Health (NIH) guidelines. Animals were purchased from Nasco (Fort Atkinson, WI, USA) at developmental stages 44-47, and raised to stages 48-49 on a 12/12 h light/dark cycle at 18 °C.

In the beginning of each experiment, a tadpole was put in a Petri dish (diameter of 10 cm) filled with 1-1.2 cm of tadpole rearing medium, placed on top of a CRT monitor with two speakers connected to the Petri dish with short wooden struts (James et al., 2015; Truszkowski et al., 2017), and kept there for 4 hours. The tadpole was visually isolated from the rest of the room with a cardboard box surrounding the apparatus. For Control and Sound groups, the monitor was on, but showed a uniform 50% gray background. For Flash, Sync and Async groups the screen showed a black-and-white checkerboard pattern, with each square in the pattern being 14 mm wide; this pattern flipped (inverted) every 1 second. For the Looming group, the inversion of the pattern was not instantaneous, but lasted for one second, with old black squares linearly shrinking into white background, and new black squares appearing and linearly expanding in the middle of each white square (Figure 1C).

The stimulation program was written in JavaScript, using the p5.js library (McCarthy et al., 2015), and is available at
http://faculty.bard.edu/~akhakhal/checker_flash_ding.html . For Sound, Sync, and Async groups a broad-spectrum sound click was delivered through the speakers every 1 second, with left and right speakers playing the same waveform, but inverted. Formally the click was generated as a 5 ms pulse of 100 Hz sine wave, but it was also distorted by the non-linearities in the system. The sound volume was calibrated to be about 2 times higher than the threshold volume, which means that it reliably evoked startle responses with about 80% success ratio, at least at the beginning for the conditioning protocol. For the Sync group, the sound clicks and the checkerboard inversions were synchronized, while for the Async group they were offset by 500 ms (half a period).

Electrophysiology

Immediately after sensory conditioning, tadpoles were anesthetized in 0.02% tricaine methanesulfanate (MS-222). Dorsal commissures were cut, the brain was dissected out (Aizenman et al., 2003; Ciarleglio et al., 2015), and placed in the recording chamber filled with artificial cerebrospinal fluid (in mM: 115 NaCl, 4 KCl, 3 CaCl2, 3 MgCl2, 5 HEPES, 10 glucose, 10 μM glycine; pH 7.2, osmolarity 255 mOsm). All chemicals were obtained from Sigma (Sigma-Aldrich, St. Louis, MO). The ventricular membrane was removed (suctioned) using a broken glass electrode. Cells were visualized with a Nikon (Tokyo, Japan) Eclipse FN1 light microscope with a 40x water immersion objective. Recordings were restricted to the middle of the tectum, as in earlier studies (Ciarleglio et al., 2015), from 25% to 53% of brain half-width medially from the lateral edge, and from 36% to 69% of tectum length rostrally from the caudal edge of the tectum (Figure 1A). Care was taken to record only from "deep" primary tectal cells (that are located superficially in our preparation), and not from MV cells (Pratt and Aizenman, 2009) or superficial layer cells (that are located deep in the tectum in our preparation) (Liu et al., 2016). Glass electrodes (1.5x0.86 mm borosilicate glass; Sutter instruments, Novato, CA) were pulled on a Sutter P-1000 puller (Sutter instruments), to a tip resistance of 8-12 MOhm. The elecrodes were filled with intracellular saline (in mM: 100 K-gluconate, 5 NaCl, 8 KCl, 1.5 MgCl2, 20 HEPES, 10 EGTA, 2 ATP, 0.3 GTP; pH 7.2, osmolarity 255 mOsm). Electrodes were placed in an Axon headstage (Molecular Devices, Sunnyvale, CA), controlled by a motorized micromanipulator (MX7600, Siskiyou, Grants Pass, OR). Whole cell patch clamp was established as usual (Ciarleglio et al., 2015), with typical final access resistance of 30 MOhm, and membrane resistance Rm of 0.33 GOhm. Signals were measured with an Axon Instruments MultiClamp 700B amplifier (Axon Instruments, Foster City, CA), filtered with a 5 kHz band-pass filter, and digitized at 10 kHz a CED Power1401-3 Digitizer (Cambridge Electronic Design; Cambridge, England). For synaptic stimulation, a bipolar stimulating electrode (Warner Instruments, Hamden, CT) was placed on the optic chiasm (Wu et al., 1996); stimuli were controlled by a CED digitizer, and were delivered by A.M.P.I. stimulus isolator (AMPI, Jerusalem, Israel).

Each neuron was subjected to a series of electrophysiological measurement protocols (see below for details), closely matching experimental protocols from (Ciarleglio et al., 2015). For each cell, we measured membrane resistance Rm and capacitance Cm in voltage clamp mode, and then (1) ran a series of voltage steps to measure ionic currents; (2) in current clamp mode, ran a series of current steps to assess cell spiking; (3) in dynamic clamp mode, subjected the cell to different conductance injections; (4) finally, if the cell was still in good health, we ran a synaptic protocol with optic chiasm stimulation. All data was processed offline using custom Matlab scripts (Mathworks, Natick, MA), and analyzed in R. In total, we recorded from 188 neurons in 35 tadpoles; of these, 159 cells had readings from all 4 protocols, while 12 lacked synaptic recordings; these 12 cells were scattered across all

6 experimental groups. After the recording was over, the position of each recorded cell was visualized with a 10x microscope, marked on a screen, measured in medial and rostral directions relative to the most latero-caudal point of the tectum, and converted into percentage (Hamodi and Pratt, 2014).

Voltage steps protocol

The baseline membrane potential was set at -60 mV (in this manuscript, the voltages are not adjusted for junction potential, which is expected to be equal to -12 mV for this combination of external and internal solutions). After Cm and Rm were measured with a standard seal test, cells were subjected to 11 voltage steps (square pulses), each 500 ms long, and 10 mV higher than the previous one, with 500 ms of baseline voltage between the steps. Each trial also contained a 50 ms long test pre-step of -10 mV relative to the baseline. During analysis, we averaged transition currents evoked by the leading and trailing edges of the pre-step, then scaled and subtracted them from the current responses to the main step. For remaining active currents, we measured average currents during a 0.4-2.7 ms range after the step (Na current), 5.7-19.7 ms after the step (Kt, or transient potassium current), and 430-490 ms (Ks, or stable potassium current). This approach is standard for recordings from the *Xenopus* tectum, as ionic currents are slow enough to be separated temporally (Aizenman et al., 2003). The ionic conductances were quantified as is (Ciarleglio et al., 2015). For each cell, the values of current as a function of voltage were fit with an empirical parametric equation:

$$I(v) = c \cdot \exp(x/b_1)/(1 + \exp(-(a - x)/b_2))$$

for Na and Kt currents (sigmoid, followed by exponential decay, inactivating), and a different equation:

$$I(v) = \max(0, \exp((x - a)/b) - e) \cdot c + d$$

for Ks current (a shifted piece of exponentially increasing curve with its lower part cut off; not inactivating). For equations with inactivation, we used its I_{max} value as a measure of amplitude, and v_a on the rising front such that $I(v_a) = I_{max}/2$ calculated the threshold potential. For curves without inactivation (Ks) we used I_{max} and the first non-zero point ($v_a = a + \log(e) \cdot b$) for the same purpose.

As a preliminary verification of our results, we compared the overall structure of our new dataset with the dataset from the 2015 study (Ciarleglio et al., 2015). The eight cellular parameters described above showed a similar pattern of coordination in both datasets: 23 pairwise correlations out of 35 total were significant ($p<0.05$) in this dataset, compared to 21 out of 35 in the 2015 study. The average absolute value of correlation coefficient was $r=0.38$ in this study, compared to $r=0.32$ in the 2015 study. This suggests that the datasets are similar and representative of true internal variability in the tectum.

Current steps protocol

For the current steps protocol, we switched each cell to current clamp mode, and adjusted the stable holding current to bring the resting membrane potential to about -60 mV. We

then subjected the cell to 10 current pulses, each 150 ms in duration, delivered every 1 s, such that currents ranged from 0 to 180 pA in 20 pA increments. Cells that did not produce at least one spike in this experiment were considered not-excitable, and were not included in the dataset. The largest number of spikes produced in response to a single current injection was estimated offline, manually, using a custom Matlab data browser that blinded the researcher to the identity of the cell. As a control, spikes were also detected automatically, using the filtering and thresholding approach that was used in (Ciarleglio et al., 2015); in 78% of cells both manual and automated estimations matched, in remaining 22% of cells the mismatch was either due to artifacts on the rising front being auto-detected as spikes, or due to spike broadening that fell below the threshold for the adaptive filter. The number of cells in which manual spike detection disagreed with automated detection did not differ across groups (6.1$\pm$1.7; p=0.5, exact Fisher test).

Dynamic clamp protocol

For dynamic clamp experiments, each cell was held at -50 mV baseline potential, and was stimulated with 5 repetitions of 12 different "conductance injections". Conductance curves were generated with a formula $G = g\frac{t}{\tau}\exp(1-\frac{t}{\tau})$, known as "alpha synapse", where g and τ are conductance and decay parameters respectively (Destexhe et al., 1994). We used four different values of τ, to represent four typical patterns of synaptic activation: 20 ms, corresponding to a total curve length (decay to 10% of the peak value) of about 100 ms, to approximate short, monosynaptic inputs (Ciarleglio et al., 2015); 40 ms, corresponding to a total curve length of about 200 ms, as for a typical in-vitro stimulus with polysynaptic activation (Xu et al., 2011); 100 ms, to mimic in-vivo inputs to the tectum in response to abrupt disappearance of light ("dark-flash") (Khakhalin et al., 2014); and 200 ms, to mimic retinal inputs in response to a 1 second-long linear looming stimulus (Khakhalin et al., 2014). Actual decay times to 10% of peak amplitude were 98, 196, 489, and 978 ms respectively. The value of g was adjusted so that conductance curves peaked at 3 target conductances of 0.2, 0.5, and 1 nS. With the cell clamped at -50 mV, these conductances would have induced currents that peaked at 10, 25, and 50 pA respectively, matching the range of peak synaptic currents observed in (Xu et al., 2011; Khakhalin et al., 2014; Ciarleglio et al., 2015). Conductance curves were always presented in the order from the shortest to the longest, and this sequence was not randomized.

For each cell, for each of 60 trials (5 repetitions of 12 conductances), spikes were counted manually, blindly, and independently by both authors, using a custom Matlab data browser script. There was a 98.5% agreement between spike number estimations on a trace-by-trace basis. All cases of disagreement (usually $\pm$1 spike) were due to later action potentials becoming broader and smaller in amplitude, which made them ambiguous. We ran sensitivity analyses of main effects reported in this paper separately on both estimations, and got qualitatively identical results. Numerically, we went with consensus numbers that in each case followed the higher estimation for the number of spikes.

To quantify the "shape" of spiking responses to conductances of different duration (temporal tuning), we encoded curve duration as an ordinal value (from 1 to 4) for every cell, fit the spike data as a function of response duration with a quadratic formula ($y = ax^2 + bx + c$), and used the quadratic coefficient a as the measure of response non-linearity. While the units and absolute values of this coefficient are not interpretable, it captures the shape of the response curve well, and allows for easy comparisons between cells (Figure 2A). The case of $a = 0$ corresponds to spiking output linearly increasing with duration increase; $a > 0$ means supralinear preference for long conductances (curving up); about $-0.25 < a < 0$ corresponds to a plateau-shaped curves, while $a < -0.25$ would mean heavy spike

inactivation for longer conductance injections.

Synaptic recordings

For synaptic recordings, we switched cells back to voltage clamp mode, and held the membrane potential at -45 mV to isolate excitatory synaptic currents. Optic chiasm shocks were delivered 10 times, every 20 s, with a stimulation strength between 0.05 and 0.4 mA, and with a pulse length of 0.2 us. In each experiment, we would first find stimulation strength that evoked consistent synaptic responses in the first cell we patched, then increased it by 20% and kept it constant for all cells recorded from that brain. Recordings were processed offline; for each trial we used the average current between 5 and 15 ms as a measure of monosynaptic response amplitude, and current between 15 and 145 ms as a measure of polysynaptic response amplitude (Ciarleglio et al., 2015). The weighted duration of synaptic responses was calculated as the "center of mass" under the first 700 ms of the curve:

$$l = \int_{0 \le t \le T} I(t)\, t\, dt \Big/ \int_{0 \le t \le T} I(t)\, dt$$

Statistics and reporting

To analyze the numbers of spikes observed in dynamic clamp experiments (Figure 1), we first averaged the number of generated spikes for each combination of conductance curve duration and amplitude, 12 values for each of 5 protocol repetitions for every cell. Then we used sequential sum of squares analysis of variance with repeated measures. Both different conductance curve amplitudes and durations were represented as ordinal values (1 to 3 for amplitude, 1 to 4 for duration). Differences between experimental groups were assessed as interactions between these ordinal values and the factor variable encoding the experimental group, as we were interested in response shapes (reflected by interactions) rather than average values of spikiness (reflected by independent terms). Cell ids were included in the analysis as a fixed factor for repeated measures analysis of variance (also equivalent to analysis of variance with blocking). To verify the validity of this approach, we also ran a maximal likelihood mixed-effects model with type III interaction terms, as implemented in R package "lmer", with "lmerTest" extension to get access to Satterthwaite degrees of freedom and p-value estimations (Kuznetsova et al., 2017). The results of both methods were numerically similar, and supported same conclusions.

For the comparison of summative descriptions of tuning, and other electrophysiological cell parameters between experimental groups, we report p-values of fixed effect sequential sum of squares linear model (ancova), in which rostral and medial coordinates of each cell within the tectum are included as covariates, and experimental group is used as the main factor. All comparisons and correlations between cell parameters are performed on values corrected for cell position within the tectum. Position correction was based on a two-way linear regression model without interaction. For five variables that were distributed extremely non-normally, this correction for position was performed on transformed values (original values were transformed to normally distributed proxy values, linearly adjusted, and then transformed back): for early and late mean synaptic amplitudes we used a transformation $a' = log(1 - a)$; for the variability of synaptic amplitudes $s' = log(1 + s)$; and for temporal tuning $y'_t = \sqrt{y_t}$. Where appropriate, we performed the analysis with and without extreme

outliers, and reported the difference. All analyses presented in the paper were also verified in mixed model analyses, with animal id included as a random factor; the results of these mixed model analyses were similar to that of a fixed model, and are not reported.

References

Aizenman, C. D., Akerman, C. J., Jensen, K. R., and Cline, H. T. (2003). Visually driven regulation of intrinsic neuronal excitability improves stimulus detection in vivo. *Neuron*, 39(5):831–842.

Aizenman, C. D. and Cline, H. T. (2007). Enhanced visual activity in vivo forms nascent synapses in the developing retinotectal projection. *Journal of neurophysiology*, 97(4):2949–2957.

Bassett, D. S. and Sporns, O. (2017). Network neuroscience. *Nature neuroscience*, 20(3):353.

Beatty, J. A., Song, S. C., and Wilson, C. J. (2014). Cell-type-specific resonances shape the responses of striatal neurons to synaptic input. *Journal of neurophysiology*, 113(3):688–700.

Bianchi, D., Marasco, A., Limongiello, A., Marchetti, C., Marie, H., Tirozzi, B., and Migliore, M. (2012). On the mechanisms underlying the depolarization block in the spiking dynamics of ca1 pyramidal neurons. *Journal of computational neuroscience*, 33(2):207–225.

Bollmann, J. H. and Engert, F. (2009). Subcellular topography of visually driven dendritic activity in the vertebrate visual system. *Neuron*, 61(6):895–905.

Brenner, N., Bialek, W., and Van Steveninck, R. d. R. (2000). Adaptive rescaling maximizes information transmission. *Neuron*, 26(3):695–702.

Ciarleglio, C. M., Khakhalin, A. S., Wang, A. F., Constantino, A. C., Yip, S. P., and Aizenman, C. D. (2015). Multivariate analysis of electrophysiological diversity of xenopus visual neurons during development and plasticity. *Elife*, 4.

Clopath, C., Büsing, L., Vasilaki, E., and Gerstner, W. (2010). Connectivity reflects coding: a model of voltage-based stdp with homeostasis. *Nature neuroscience*, 13(3):344.

Deeg, K. E., Sears, I. B., and Aizenman, C. D. (2009). Development of multisensory convergence in the xenopus optic tectum. *Journal of Neurophysiology*, 102(6):3392–3404.

Destexhe, A., Mainen, Z. F., and Sejnowski, T. J. (1994). Synthesis of models for excitable membranes, synaptic transmission and neuromodulation using a common kinetic formalism. *Journal of computational neuroscience*, 1(3):195–230.

Dong, W., Lee, R. H., Xu, H., Yang, S., Pratt, K. G., Cao, V., Song, Y.-K., Nurmikko, A., and Aizenman, C. D. (2009). Visual avoidance in xenopus tadpoles is correlated with the maturation of visual responses in the optic tectum. *Journal of neurophysiology*, 101(2):803–815.

Drion, G., O'Leary, T., and Marder, E. (2015). Ion channel degeneracy enables robust and tunable neuronal firing rates. *Proceedings of the National Academy of Sciences*, 112(38):E5361–E5370.

Evans, M. D., Dumitrescu, A. S., Kruijssen, D. L., Taylor, S. E., and Grubb, M. S. (2015). Rapid modulation of axon initial segment length influences repetitive spike firing. *Cell reports*, 13(6):1233–1245.

Felch, D. L., Khakhalin, A. S., and Aizenman, C. D. (2016). Multisensory integration in the developing tectum is constrained by the balance of excitation and inhibition. *Elife*, 5.

Fiete, I. R., Senn, W., Wang, C. Z., and Hahnloser, R. H. (2010). Spike-time-dependent plasticity and heterosynaptic competition organize networks to produce long scale-free sequences of neural activity. *Neuron*, 65(4):563–576.

Frank, H. Y. and Catterall, W. A. (2003). Overview of the voltage-gated sodium channel family. *Genome biology*, 4(3):207.

Goldwyn, J. H., Slabe, B. R., Travers, J. B., and Terman, D. (2018). Gain control with a-type potassium current: Ia as a switch between divisive and subtractive inhibition. *arXiv preprint arXiv:1802.04794*.

Grubb, M. S. and Burrone, J. (2010). Activity-dependent relocation of the axon initial segment fine-tunes neuronal excitability. *Nature*, 465(7301):1070.

Hamada, M. S., Goethals, S., de Vries, S. I., Brette, R., and Kole, M. H. (2016). Covariation of axon initial segment location and dendritic tree normalizes the somatic action potential. *Proceedings of the National Academy of Sciences*, 113(51):14841–14846.

Hamodi, A. S., Liu, Z., and Pratt, K. G. (2016). An nmda receptor-dependent mechanism for subcellular segregation of sensory inputs in the tadpole optic tectum. *eLife*, 5.

Hamodi, A. S. and Pratt, K. G. (2014). Region-specific regulation of voltage-gated intrinsic currents in the developing optic tectum of the xenopus tadpole. *Journal of neurophysiology*, 112(7):1644–1655.

Hildebrand, D. G. C., Cicconet, M., Torres, R. M., Choi, W., Quan, T. M., Moon, J., Wetzel, A. W., Champion, A. S., Graham, B. J., Randlett, O., et al. (2017). Whole-brain serial-section electron microscopy in larval zebrafish. *Nature*, 545(7654):345.

Hiramoto, M. and Cline, H. T. (2009). Convergence of multisensory inputs in xenopus tadpole tectum. *Developmental neurobiology*, 69(14):959–971.

James, E. J., Gu, J., Ramirez-Vizcarrondo, C. M., Hasan, M., Truszkowski, T. L., Tan, Y., Oupravanh, P. M., Khakhalin, A. S., and Aizenman, C. D. (2015). Valproate-induced neurodevelopmental deficits in xenopus laevis tadpoles. *Journal of Neuroscience*, 35(7):3218–3229.

Jang, E. V., Ramirez-Vizcarrondo, C., Aizenman, C. D., and Khakhalin, A. S. (2016). Emergence of selectivity to looming stimuli in a spiking network model of the optic tectum. *Frontiers in neural circuits*, 10:95.

Jarvis, S., Nikolic, K., and Schultz, S. R. (2018). Neuronal gain modulability is determined by dendritic morphology: A computational optogenetic study. *PLoS computational biology*, 14(3):e1006027.

Khakhalin, A. S. and Aizenman, C. D. (2012). Gabaergic transmission and chloride equilibrium potential are not modulated by pyruvate in the developing optic tectum of xenopus laevis tadpoles. *PLoS One*, 7(4):e34446.

Khakhalin, A. S., Koren, D., Gu, J., Xu, H., and Aizenman, C. D. (2014). Excitation and inhibition in recurrent networks mediate collision avoidance in xenopus tadpoles. *European Journal of Neuroscience*, 40(6):2948–2962.

Kole, M. H., Letzkus, J. J., and Stuart, G. J. (2007). Axon initial segment kv1 channels control axonal action potential waveform and synaptic efficacy. *Neuron*, 55(4):633–647.

Kole, M. H. and Stuart, G. J. (2012). Signal processing in the axon initial segment. *Neuron*, 73(2):235–247.

Kuba, H., Oichi, Y., and Ohmori, H. (2010). Presynaptic activity regulates na+ channel distribution at the axon initial segment. *Nature*, 465(7301):1075.

Kuznetsova, A., Brockhoff, P. B., and Christensen, R. H. (2017). lmertest package: Tests in linear mixed effects models. *Journal of Statistical Software*, 82(13):1–26.

Leterrier, C. (2018). The axon initial segment: an updated viewpoint. *Journal of Neuroscience*, 38(9):2135–2145.

Liu, Z., Ciarleglio, C. M., Hamodi, A. S., Aizenman, C. D., and Pratt, K. G. (2016). A population of gap junction-coupled neurons drives recurrent network activity in a developing visual circuit. *Journal of neurophysiology*, 115(3):1477–1486.

Lukoševičius, M. and Jaeger, H. (2009). Reservoir computing approaches to recurrent neural network training. *Computer Science Review*, 3(3):127–149.

Marcelin, B., Chauvière, L., Becker, A., Migliore, M., Esclapez, M., and Bernard, C. (2009). H channel-dependent deficit of theta oscillation resonance and phase shift in temporal lobe epilepsy. *Neurobiology of disease*, 33(3):436–447.

Marder, E. and Taylor, A. L. (2011). Multiple models to capture the variability in biological neurons and networks. *Nature neuroscience*, 14(2):133.

McCarthy, L., Reas, C., and Fry, B. (2015). *Getting Started with P5. js: Making Interactive Graphics in JavaScript and Processing*. Maker Media, Inc.

Narayanan, R. and Johnston, D. (2008). The h channel mediates location dependence and plasticity of intrinsic phase response in rat hippocampal neurons. *Journal of Neuroscience*, 28(22):5846–5860.

O'Leary, T., Williams, A. H., Caplan, J. S., and Marder, E. (2013). Correlations in ion channel expression emerge from homeostatic tuning rules. *Proceedings of the National Academy of Sciences*, 110(28):E2645–E2654.

Picton, L. D., Sillar, K. T., and Zhang, H.-Y. (2018). Control of xenopus tadpole locomotion via selective expression of ih in excitatory interneurons. *Current Biology*.

Popovic, M. A., Foust, A. J., McCormick, D. A., and Zecevic, D. (2011). The spatio-temporal characteristics of action potential initiation in layer 5 pyramidal neurons: a voltage imaging study. *The Journal of physiology*, 589(17):4167–4187.

Pratt, K. G. and Aizenman, C. D. (2007). Homeostatic regulation of intrinsic excitability and synaptic transmission in a developing visual circuit. *Journal of Neuroscience*, 27(31):8268–8277.

Pratt, K. G. and Aizenman, C. D. (2009). Multisensory integration in mesencephalic trigeminal neurons in xenopus tadpoles. *Journal of neurophysiology*, 102(1):399–412.

Pratt, K. G., Dong, W., and Aizenman, C. D. (2008). Development and spike timing–dependent plasticity of recurrent excitation in the xenopus optic tectum. *Nature neuroscience*, 11(4):467.

Pratt, K. G. and Khakhalin, A. S. (2013). Modeling human neurodevelopmental disorders in the xenopus tadpole: from mechanisms to therapeutic targets. *Disease models & mechanisms*, pages dmm–012138.

Prinz, A. A., Abbott, L., and Marder, E. (2004a). The dynamic clamp comes of age. *Trends in neurosciences*, 27(4):218–224.

Prinz, A. A., Bucher, D., and Marder, E. (2004b). Similar network activity from disparate circuit parameters. *Nature neuroscience*, 7(12):1345.

Reimann, M. W., Nolte, M., Scolamiero, M., Turner, K., Perin, R., Chindemi, G., Dłotko, P., Levi, R., Hess, K., and Markram, H. (2017). Cliques of neurons bound into cavities provide a missing link between structure and function. *Frontiers in computational neuroscience*, 11:48.

Rubinov, M., Sporns, O., Thivierge, J.-P., and Breakspear, M. (2011). Neurobiologically realistic determinants of self-organized criticality in networks of spiking neurons. *PLoS computational biology*, 7(6):e1002038.

Shen, W., McKeown, C. R., Demas, J. A., and Cline, H. T. (2011). Inhibition to excitation ratio regulates visual system responses and behavior in vivo. *Journal of neurophysiology*, 106(5):2285–2302.

Spruston, N., Jaffe, D. B., Williams, S. H., and Johnston, D. (1993). Voltage-and space-clamp errors associated with the measurement of electrotonically remote synaptic events. *Journal of Neurophysiology*, 70(2):781–802.

Stein, B. E., Stanford, T. R., and Rowland, B. A. (2014). Development of multisensory integration from the perspective of the individual neuron. *Nature Reviews Neuroscience*, 15(8):520.

Stemmler, M. and Koch, C. (1999). How voltage-dependent conductances can adapt to maximize the information encoded by neuronal firing rate. *Nature neuroscience*, 2(6):521.

Takemura, S.-y. (2014). Connectome of the fly visual circuitry. *Microscopy*, 64(1):37–44.

Tien, N.-W. and Kerschensteiner, D. (2018). Homeostatic plasticity in neural development. *Neural development*, 13(1):9.

Titley, H. K., Brunel, N., and Hansel, C. (2017). Toward a neurocentric view of learning. *Neuron*, 95(1):19–32.

Truszkowski, T. L., Carrillo, O. A., Bleier, J., Ramirez-Vizcarrondo, C. M., Felch, D. L., McQuillan, M., Truszkowski, C. P., Khakhalin, A. S., and Aizenman, C. D. (2017). A cellular mechanism for inverse effectiveness in multisensory integration. *Elife*, 6.

Turrigiano, G. (2011). Too many cooks? intrinsic and synaptic homeostatic mechanisms in cortical circuit refinement. *Annual review of neuroscience*, 34:89–103.

Venables, W. N. and Ripley, B. D. (2013). *Modern applied statistics with S-PLUS*. Springer Science & Business Media.

Wu, G.-Y., Malinow, R., and Cline, H. (1996). Maturation of a central glutamatergic synapse. *Science*, 274(5289):972–976.

Xu, H., Khakhalin, A. S., Nurmikko, A. V., and Aizenman, C. D. (2011). Visual experience-dependent maturation of correlated neuronal activity patterns in a developing visual system. *Journal of Neuroscience*, 31(22):8025–8036.